Contactless power supply for magnetically levitated elevator systems

R. Appunn, B. Riemer and Kay Hameyer

***Abstract*—Magnetically levitated vehicles need a contactless energy transmission system to supply on-board components without physical contact to a guiding rail. In contrast to stand-alone contactless power supply (CPS) systems this paper introduces a combined CPS and electromagnetic guiding system (MGS). The inductive energy transmission is realized by utilizing the magnetic circuit of an actuator of the linear guiding. With this approach two devices are combined into one entity. The hybrid actuator consists of an omega shape iron yoke with permanent magnets and coils on its lateral arms. A concentrated primary winding is added to the guide rail and a coil wound around the cetral arm of the omega actuator functions as secondary winding. Hereby a superposition of the MGS flux and the CPS flux emerges in the magnetic circuit of the actuator and the transmission path is established. The proposed system requires less construction space and weight compared to existing energy transmission systems.**

***Index Terms*—Contactless power supply, control, hybrid actuator, inductive energy transmission, linear guiding, magnetic levitation (maglev), simulation**

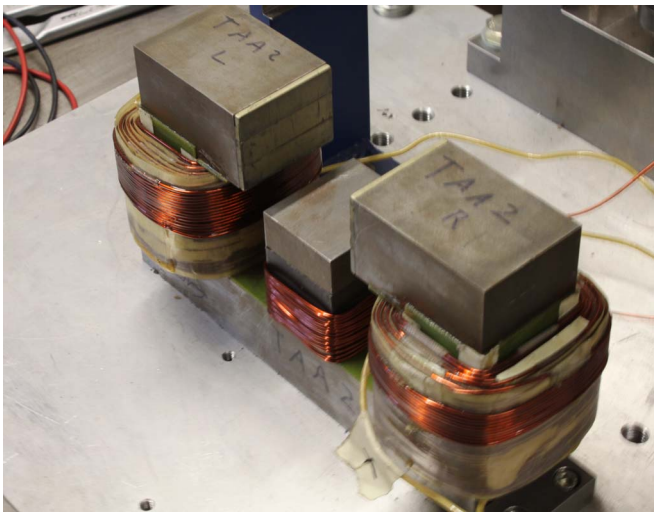

Fig. 1. Omega actuator on test bench.

NOMENCLATURE

γ	Electric conductivity
μ	Magnetic permeability
μ_r	Relative permeability
ω_0	Angular freqency of the CPS
Ψ_p	Flux linkage of the primary coil
Ψ_s	Flux linkage of the secondary coil
B_m	Mean magnetic flux density
C_p	Primary capacitance
C_s	Secondary capacitance
d	Length of a PM plate
F_x	Pulling force in x direction
F_y	Pulling force in y direction
k	Inverse skin depth
k_{CPS}	Coupling coefficient
L_p	Primary self inductance
L_s	Secondary self inductance
M	Mutual inductance
P_s	Transmittable electric power
Q_p	Primary quality factor
Q_s	Secondary quality factor
R_L	Load resistance
R_p	Primary coil resistance
R_s	Secondary coil resistance
V	Volume of a PM plate
Z_f	Transformed equivalent impedance of the secondary

I. INTRODUCTION

Contactless power transmission is of particular interest for electromagnetically levitated vehicles. The ability to transfer energy from a fixed guide way to the moving part without sliding contacts or traveling cables augments their benefits such as wearless operation. Electromagnetically levitated trains or other fast moving vehicles are able to consume power via harmonics induced by the propulsion device mounted to the guide way [1]–[3]. For slow vehicles, such as elevators with linear drives [4]–[7], this concept does not suite, because an extra induction rail in the guide way and additional coils on the vehicle have to be constructed. In automotive systems one can find similar approaches [8], [9]. This yields extra cost and requires additional construction space.

Previous studies to minimize both, cost and space, are based on an integrated solution of guiding and power transmission [10]. In this paper a similar strategy is followed. On the central arm of one electromagnetic omega shaped actuator of the MGS depicted in figure 1 an additional coil with 14 windings is placed. This coil functions as secondary winding for the energy transmission system. A concentrated coil, consisting of seven windings is placed into a slot embedded within laminated steel on the guide rail (figure 4). It produces a high frequent electromagnetic field, which superposes the levitating field. Hereby, a voltage is induced in the secondary coils mounted to the moving part and the power supply of the vehicle is established. Thereby, an integrated solution for both, contactless guiding and contactless power transmission using existing components is found. Figure 2 shows the topology.

The guiding system consists of four omega actuators with two coils on each actuator [11] using a degree of freedom (DOF) control [12] for the translatory and rotatory DOF of the elevator car. The design and control of the MGS are described in detail in [13]. The power transmission is designed to enhance the IEM elevator test bench in scale of 1:6 [14].

Institute of Electrical Machines (IEM), RWTH Aachen University, Schinkelstr. 4, D-52056 Aachen, Germany

978-1-4673-0142-8/12/$26.00 ©2012 IEEE

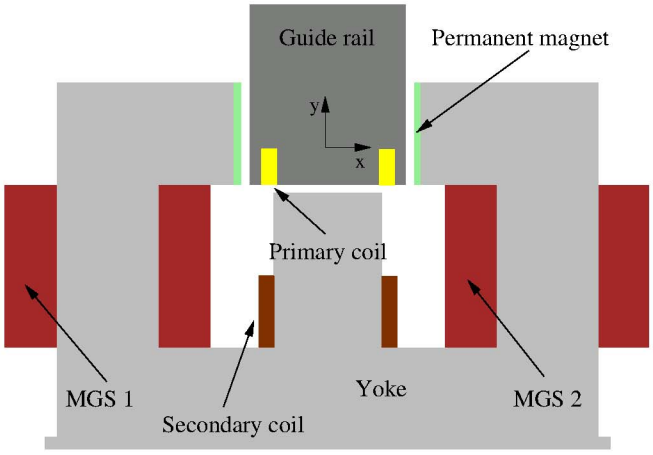

Fig. 2. Omega actuator with CPS.

A nominal load of 200 W has to be transferred to supply the MGS coils and the on-board electronic components in the cabin such as eddy current sensors and current controllers.

The general structure of the contactless power transmission system is presented in figure 3. Starting from a DC link an inverter topology generates a high frequent sinusoidal current. After primary reactive power compensation the transmission path i.e. the actuator entity is used. A secondary compensation follows hereafter. The voltage adjustment for the load is done by an active voltage control.

II. Contacless power supply

A. Modeling of the transmission path

The contactless power transmission utilizes an electromagnetic flux created by the primary conductor embedded within laminated steel in the guide rail, passing through the ferromagnetic yoke and guide rail, the permanent magnets and the air gaps. It induces an electromotive force in the secondary coil as well as the MGS coils. In the studied scenario the secondary coil is used for energy transmission, only.

1) Theoretical framework: Describing the transmission path as a transformer leads to the following differential equation system (compare figure 8):

$$\begin{pmatrix} u_p \\ u_s \end{pmatrix} = \begin{pmatrix} R_p & 0 \\ 0 & R_s \end{pmatrix} \begin{pmatrix} i_p \\ i_s \end{pmatrix} + \partial_t \begin{pmatrix} \Psi_p \\ \Psi_s \end{pmatrix} \tag{1}$$

with the winding resistances $R_{p,s}$. The time-derivative of the flux linkages is given by:

$$\partial_t \begin{pmatrix} \Psi_p \\ \Psi_s \end{pmatrix} = \partial_{\mathrm{i}} \begin{pmatrix} \Psi_p \\ \Psi_s \end{pmatrix} \cdot \partial_t \begin{pmatrix} i_p \\ i_s \end{pmatrix}. \tag{2}$$

In the range of operation of the considered CPS system the ferromagnetic material is not saturated. Therefore the derivative $\partial_{\mathrm{i}} \boldsymbol{\Psi}$ is constant, this yields:

$$\partial_{\mathrm{i}} \begin{pmatrix} \Psi_p \\ \Psi_s \end{pmatrix} = \mathbf{L} = \begin{pmatrix} L_p & -M \\ -M & L_s \end{pmatrix}. \tag{3}$$

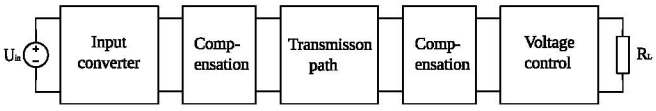

Fig. 3. Components of the power transmission system.

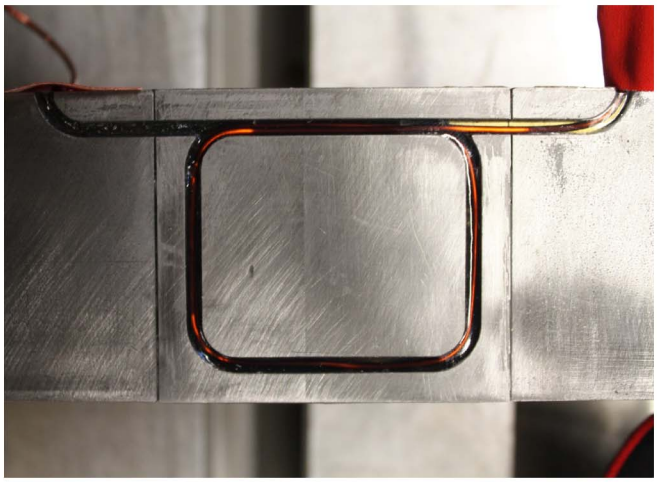

Fig. 4. Primary coil embedded within guide rail.

$\mathbf{L}$ is the inductance matrix including all self and mutual inductances.

To determine the inductance matrix with an adequate accuracy to investigate the power transmission capability of the system, the matrix is extracted by means of the finite element method. The inductances are extracted as described in [15]. Because of the linear B-H characteristic in the range of operation the tangent inductance matrix is equal to the secant one [15]. To consider the different axial length of the long guide rail and the short omega actuator it is not sufficient to create a 2D FE model. Hence a 3D FE model of the actuator (figure 5) is generated. Once the inductance matrix is extracted for the linear case all points of operation can be calculated analytically in the same accuracy as performed by a computational FE computation. A coupling of the FE model to the circuit simulator is not required. The inductance matrix of the considered actuator is given in table I.

Since the elevator car is not always at equilibrium position in the center of the shaft, the air gaps between actuator and guide rail vary in range of several μm. This results in a variation of the mutual inductance M. Figure 6 depicts M with respect to a local displacement in x and y direction. A variation of 12 μH is simulated according to a spatial displacement of 1 mm. Under normal operation the air gap variation is less than 50 μm, so the deviation is tolerated.

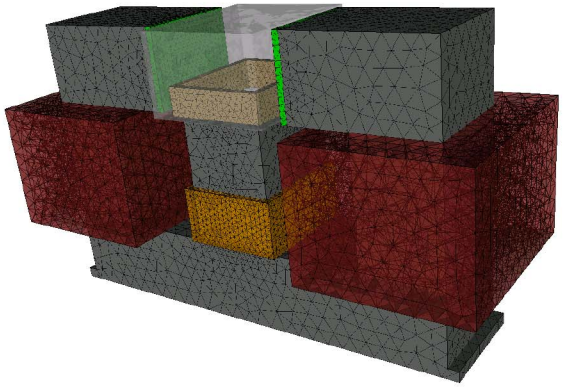

Fig. 5. FE model of the actuator.

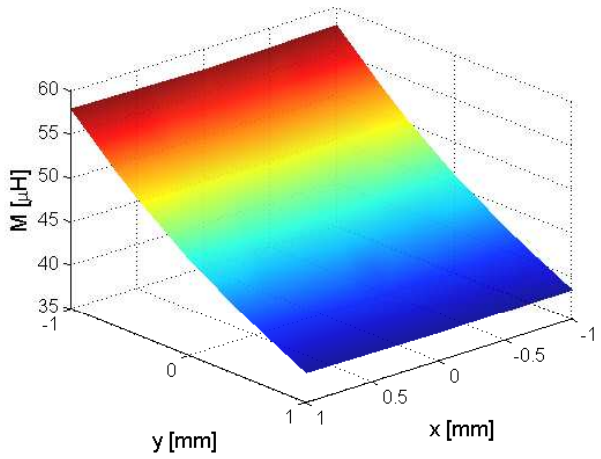

Fig. 6. Mutual inductance variation.

B. Measurements of the inductance matrix

Hereafter the inductances are measured at the omega actuator test bench (figure 1). From no-load measurements, powering primary and afterwards secondary coil the impedances and thereby the self inductances of each coil and the mutual inductance can be determined (Table I). The deviation of L_p is within measurement tolerances. The deviation of the mutual inductance and the secondary self inductance can be explained by imprecise determination of material characteristic at operating frequency. The relative permeability μ_r of the laminated steel is measured in an Epstein test frame at different frequency. Figure 7 shows the falling characteristic of μ_r with increasing frequency. At 10 kHz a $\mu_r = 784$ is measured. But this is only valid applying a homogeneous magnetic field as in the test frame. In the actuator the direction of the magnetic flux depends on the local position in the yoke. The permeability of the permanent magnet material is uncertain at this frequency either. Furthermore a slight displacement of the air gaps at the test bench results in deviations of the mutual inductance, since the magnetic circuit is changed (compare figure 6).

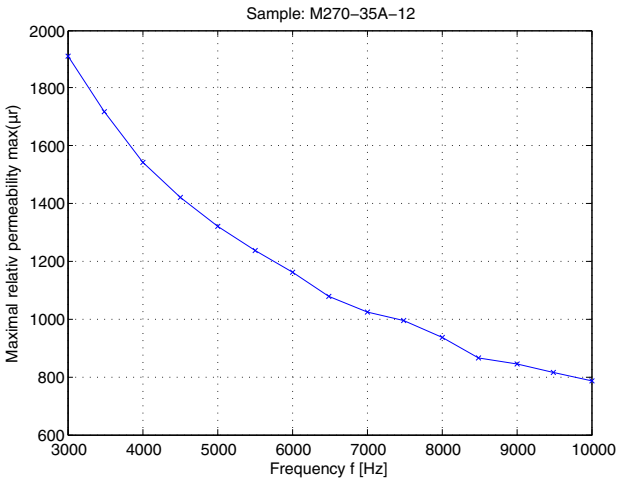

Fig. 7. Measured relative permeability of laminated steel.

TABLE I
PARAMETER OF THE INDUCTANCE MATRIX DESCRIBING THE MUTUAL INDUCTORS.

Inductance	simulated	measured	deviation
$L_p[\mu H]$	46.9	46	1.9 %
$L_s[\mu H]$	186	144	22.5 %
$M[\mu H]$	45.6	36.6	20 %

C. Reactive power compensation

Due to the inductances of primary and secondary windings the impedance of the transmission path has a significant inductive component. To avoid transmitting high reactive power, a power factor correction is required. Capacitances have to be added to the primary and the secondary circuit. Various topologies can be found in literature [16]. A series compensation on both sides (serial-serial-topology) is the most appropriate topology for the transmission path. In this case the secondary side has a voltage source characteristic and the reflected impedance has no imaginary part at resonance frequency. Herby the primary capacitance can be designed independently of the mutual inductance M and the coupling factor k_{cps} respectively [17].

The magnetic coupling can be characterized by the coupling coefficient,

$$k_{CPS} = \frac{M}{\sqrt{L_s \cdot L_p}}. \tag{4}$$

In contrast to transformers, and due to the relative large air gap, the coupling coefficient of contactless power supply systems is much smaller.

At resonant frequency ω_0 the reactances of a series resonance circuit are defined at

$$X = X_L + X_C = \omega_0 L - \frac{1}{\omega_0 C} = 0. \tag{5}$$

With given inductances L_p and L_s, the required capacitances are

$$C_p = \frac{1}{L_p \cdot {\omega_0}^2}, \tag{6}$$

$$C_s = \frac{1}{L_s \cdot {\omega_0}^2}. \tag{7}$$

The quality factors of primary and secondary side are further important characteristics. For a series-series topology they are defined as

$$Q_p = \frac{L_p \cdot \omega_0}{Z_f} = \frac{L_p \cdot R_L}{M^2 \cdot \omega_0}, \tag{8}$$

$$Q_s = \frac{L_s \cdot \omega_0}{R_L}. \tag{9}$$

Here R_L is the load resistance at secondary side. Z_f is the transformed equivalent impedance of the secondary

$$Z_f = \frac{M^2 \cdot {\omega_0}^2}{R_L}. \tag{10}$$

The ratio of Q_p and Q_s is an indicator for the system stability [18]. $Q_p \gg Q_s$ should be aspired. With increasing length of the primary conductor Q_p is increasing, as well. The transmittable electric power can be calculated using the reflected impedance [17] defined in equation (10)

$$P_s = Re\{Z_f\} \cdot I_p^2 = I_p^2 \cdot \frac{M^2 \cdot {\omega_0}^2}{R_L}. \tag{11}$$

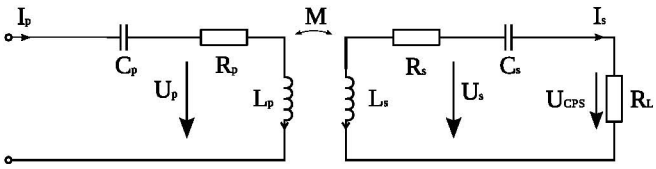

Fig. 8. Equivalent circuit of the transmission path.

With the equation of the secondary quality factor (9) we get

$$P_s = I_p^2 \cdot \frac{M^2 \cdot \omega_0 \cdot Q_s}{L_s}. \tag{12}$$

The transmittable power depends quadratically on the primary current I_p and the mutual inductance M. A poor magnetic coupling can be compensated by a high primary current. The transmission path including load resistance and compensation is depicted in figure 8.

D. computation of losses

To determine the efficiency of the proposed inductive power transmission system a brief analysis of the different losses has to be done. Ohmic losses arise in the primary and secondary windings, whereas eddy current losses exist in the laminated steel of the actuator and the permanent magnets. Due to the offset magnetization of the iron circuit, resulting from the permanent magnets and the low amplitude of the magnetic flux density the hysteresis losses are neglected.

1) Coils: The measured resistances of primary and secondary coil are $16.57m\Omega$ and $28.25m\Omega$, respectively. With this values the ohmic power dissipation of the coils is less than 5W. Skin and proximity effect are neglected since the skin depth of copper at operating frequency of 10kHz is 0.67mm which is equals the radius of the selected wire.

2) Laminations: Resulting from a high frequent alternating magnetic field, eddy current losses occur in the flux guiding parts of the actuator. Therefore the actuator and the part of the guide rail where the primary conductor is placed are fabricated of laminated steel. By finite element calculation the amplitude of the magnetic flux density B in actuator and guide rail is determined to be 0.02 Tesla. On an Epstein test frame a magnetic field of 10 kHz is applied to the laminations inducing the simulated flux density. Losses of $1.77\frac{W}{kg}$ are measured.

3) Permanent magnets: The permanent magnet material on the lateral arms of the actuator is NdFeB. The conductivity of this rare earth material is not negligible. The eddy current losses in the magnets are calculated analytically [19]. Figure 9 defines the vectors of induction and current density and the geometrical parameters of the considered PM. The losses within the pm plate can be described with the following equation:

$$P = \frac{1}{24}\gamma\ \omega^2 d^2 B_m^2 V \frac{3}{kd} = \frac{\sqrt{2}}{8}\sqrt{\frac{\gamma\omega^3}{\mu}} d B_m^2 V. \tag{13}$$

Where γ is the electric conductivity, k the inverse skin depth, μ the permeability, B_m the mean magnetic flux density and V the volume of the plate. A reduction of the losses within the permanent magnet can be achieved by segmentation of the magnet plates. Using 10 plates with a length of $d = 5mm$ resulting in eddy current losses of 4.64 W.

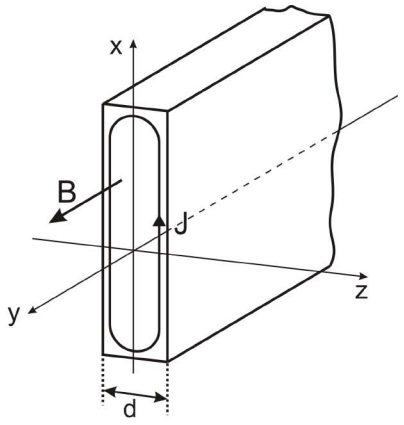

Fig. 9. Current density in a permanent magnet.

III. Simulation Results

Using the Piece-wise Linear Electric Circuit Simulation software PLECS [20], dynamic system simulation in Matlab/Simulink is performed. Hereby the control circuits can be described in a signal orientated environment, whereas the electrical quantities are described by equivalent circuits with concentrated parameters. Several load cases and the interaction with the magnetic guiding system is simulated. Figure 10 shows the output quantities i.e. voltage, current and output power, supplying a load resistance of 4Ω in steady state operation. The induced voltage reaches 40 V oscillating at 10 kHz. The current amplitude is 10 A. The instantaneous power oscillates at double operation frequency around 200 W. The simulated mean values of input and output power are presented in figure 11. Here a load change from 0 W to 200 W at 0.05 s is shown. Output and input power have the same shape. The load changes resemble the power demands of the coils, during operation of the MGS. Here only ohmic losses are regarded, which explains the small deviation of the values. The aforementioned eddy current losses, occurring in the laminations and permanent magnets, have to be added, resulting in an overall efficiency of $\sim 80\%$.

IV. Force Computation

The integration of the primary coil into the guide rail means a virtual increase of the air gap between actuator and rail, since the magnetic permeability of copper equals

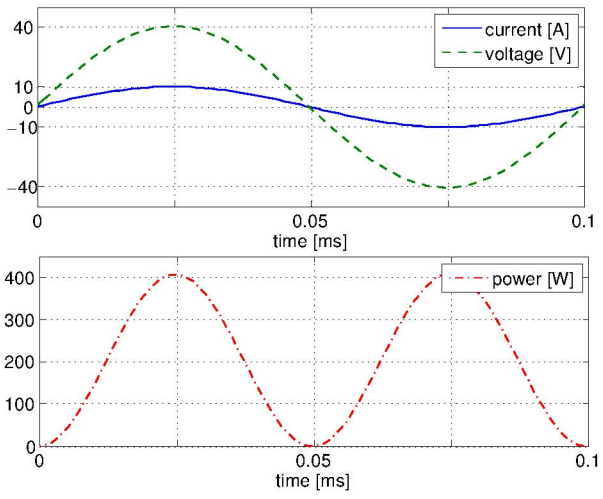

Fig. 10. Steady state output quantities of the contactless power supply.

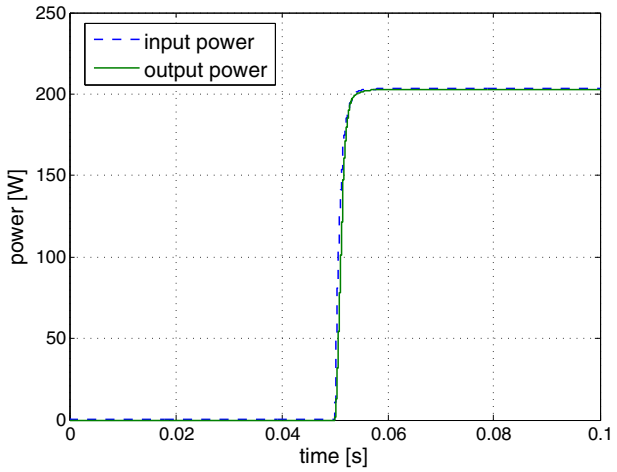

Fig. 11. Input and output power during load change.

air. Therefore a numerical analysis of the resulting pulling forces in x and y direction has been done. Regarding table II a small force drop compared to the topology without primary coil occurs. As it can be seen the difference is negligible and full operation of the guiding system is achieved. Several load conditions of the MGS coils and several displacements of the ω-actuator to the guide rail are simulated. Figures 12-16 show the resulting pulling forces in x and y direction. The nominal forces of 400N in equilibrium position can be achieved. Depending on the current in the coils and the air gap displacement different forces can be created. 2000 At is the maximum magnetomotive force of each coil.

TABLE II
COMPARISON OF PULLING FORCES.

coil currents [At]	direction	original [N]	with primary coil [N]	deviation [%]
N1,N2=0	x	0	0	0
	y	100	98	2
N1,N2=2000	x	0	0	0
	y	452.6	442.1	2.3
N1,N2=-2000	x	0	0	0
	y	4.3	4.6	6.5
N1=2000	x	384.4	380.2	1.1
N1=-2000	y	101	99.4	1.6

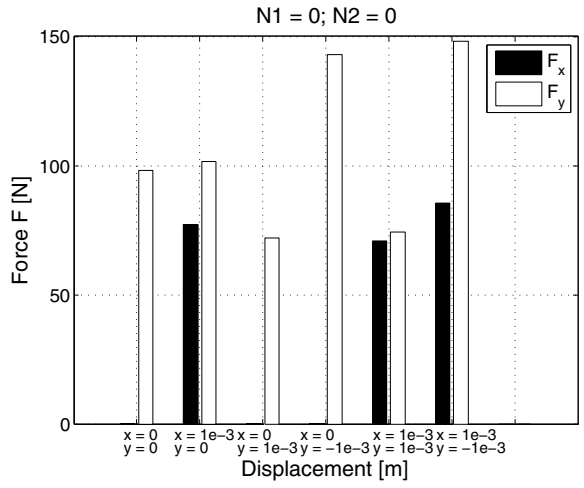

Fig. 12. Simulated forces with no current suplied.

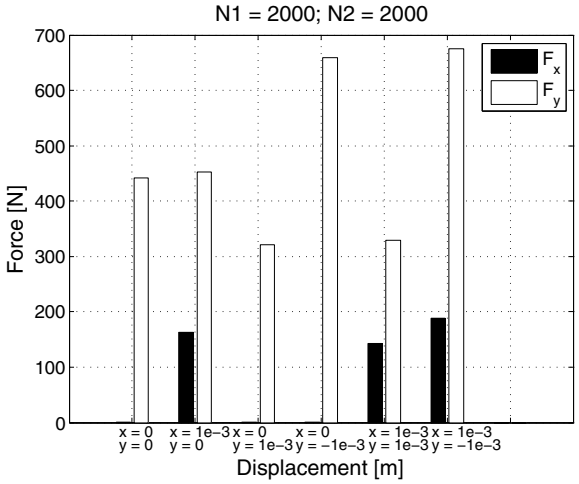

Fig. 13. Simulated forces in x-direction with positive current suplied.

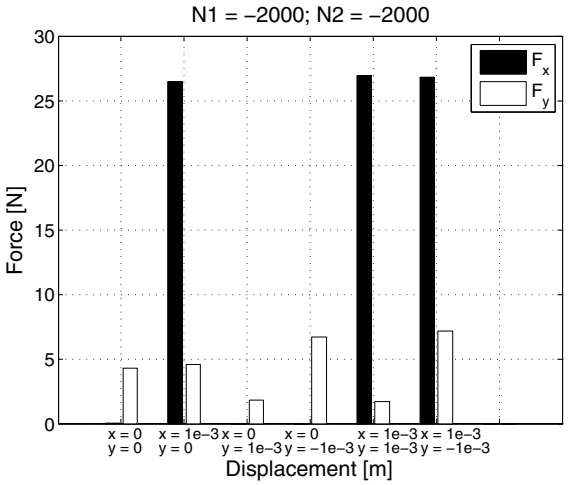

Fig. 14. Simulated forces in x-direction with negative current suplied.

V. CONCLUSIONS

This paper focuses on a combined magnetic guiding system and contactless power supply actuator entity for a vertical transportation vehicle. This topology augments the benefits of an elevator with a linear drive by eliminating any physical contact to the shaft. The same magnetic flux path in the actuator yoke is used for inductive power supply and magnetic guiding. Hereby construction space and costs can be reduced. The modeling of the inductive transmission path is done by concentrated parameters extracted from finite element analysis. On a test bench the parameters are measured and a good match between simulation and measurement can be seen. The effect of the additional CPS coil on the guiding forces is analyzed in detail. The operation of the linear guiding is verified. Losses are determined by analytical models and by measurement. Numerical loss calculation using finite element analysis and further measurements including load operation and the interaction with the guiding system will be presented in future works.

REFERENCES

[1] J.-Y. Lee, I.-J. Lee, J.-W. Kim, J.-H. Chang, D.-H. Kang, S.-U. Chung, and J.-P. Hong, “Contactless power transfer system combined with

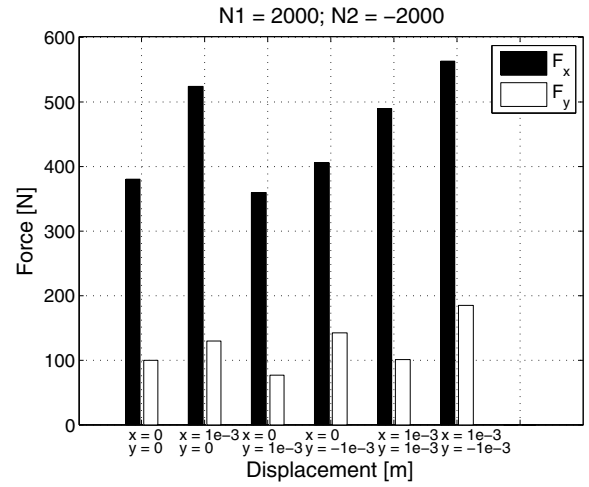

Fig. 15. Simulated forces in x-direction with pos/neg current suplied.

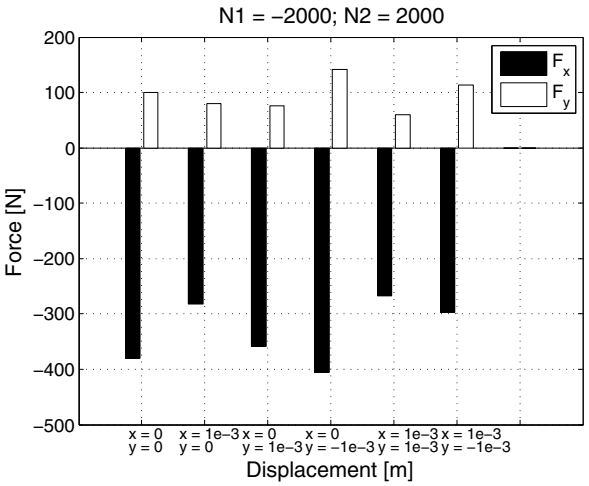

Fig. 16. Simulated forces in y-direction with neg/pos current suplied.

linear electric machine," in *Electrical Machines and Systems, 2007. ICEMS. International Conference on*, 2007, pp. 1544 –1548.

[2] G. Liang, D. Hao, and L. Qinfen, "Character analysis and optimized design of linear motor in maglev trains," in *Electrical Machines and Systems (ICEMS), 2010 International Conference on*, oct. 2010, pp. 1542 –1545.

[3] M. Chen, D. Zhou, D. Xu, and X. Wu, "Study of maximum linear generator output power for maglev emergency power supply," in *Applied Power Electronics Conference and Exposition, 2005. APEC 2005. Twentieth Annual IEEE*, vol. 3, march 2005, pp. 2036 – 2041 Vol. 3.

[4] M. Platen and G. Henneberger, "Examination of leakage and end effects in a linear synchronous motor for vertical transportation by means of finite element computation," *IEEE Transactions on Magnetics*, vol. 37, no. 5, pp. 3640–3643, September 2001.

[5] H. S. Lim, R. Krishnan, and N. S. Lobo, "Design and control of a linear propulsion system for an elevator using linear switched reluctance motor drives," *IEEE Transactions on Industrial Electronics*, vol. 55, no. 2, pp. 534–542, Febuary 2008.

[6] H. S. Lim and R. Krishnan, "Ropeless elevator with linear switched reluctance motor drive actuation systems," *IEEE Transactions on Industrial Electronics*, vol. 54, no. 4, pp. 2209–2218, August 2007.

[7] N. S. Lobo, H. S. Lim, and R. Krishnan, "Comparison of linear switched reluctance machines for vertical propulsion application: Analysis, design, and experimental correlation," *IEEE Transactions on Industry Applications*, vol. 44, no. 4, pp. 1134–1142, August 2008.

[8] J. Sallan, J. L. Villa, A. Llombart, and J. F. Sanz, "Optimal design of icpt systems applied to electric vehicle battery charge," *IEEE Transactions on Industrial Electronics*, vol. 56, no. 6, pp. 2140–2149, June 2009.

[9] G. Covic, J. Boys, M. Kissin, and H. Lu, "A three-phase inductive power transfer system for roadway-powered vehicles," *IEEE Transactions on Industrial Electronics*, vol. 54, no. 6, pp. 3370–3378, Dec. 2007.

[10] B. Schmülling and K. Hameyer, "PowerTRACE - a Novel Power Transmission and Actuator Entity," in *20th International Conference on Magnetically Levitated Systems and Linear Drives, MAGLEV*, San Diego, USA, December 2008, pp. 15–18.

[11] M. Morishita and M. Akashi, "Electromagnetic non-contact guide system for elevator cars," in *The Third International Symposium on Linear Drives for Industry Applications*. Nagano, Japan: LDIA, October 2001, pp. 416–419.

[12] A. S. Ghersin and R. S. Sánchez Peña, "LPV Control of a 6-DOF Vehicle," *IEEE Transactions on Control Systems Technology*, vol. 10, no. 6, pp. 883–887, November 2002.

[13] R. Appunn, B. Schmülling, and K. Hameyer, "Electromagnetic Guiding of Vertical Transportation Vehicles: Experimental Evaluation," *IEEE Trans. on Industrial Electronics*, vol. 57, no. 1, pp. 335–343, January 2010.

[14] R. Appunn and K. Hameyer, "Redundancy aspects of an electromagnetic guiding system for a vertical transportation vehicle," in *The 21st International Conference on Magnetically Levitated Systems and Linear Drives, MAGLEV 2011*, 2011.

[15] E. Lange, F. Henrotte, and K. Hameyer, "An efficient field-circuit coupling based on a temporary linearization of fe electrical machine models," *Magnetics, IEEE Transactions on*, vol. 45, no. 3, pp. 1258 –1261, 2009.

[16] C.-S. Wang, O. Stielau, and G. Covic, "Design considerations for a contactless electric vehicle battery charger," *Industrial Electronics, IEEE Transactions on*, vol. 52, no. 5, pp. 1308 – 1314, 2005.

[17] C.-S. Wang, G. Covic, and O. Stielau, "Power transfer capability and bifurcation phenomena of loosely coupled inductive power transfer systems," *Industrial Electronics, IEEE Transactions on*, vol. 51, no. 1, pp. 148 – 157, 2004.

[18] J. Boys, G. Covic, and A. Green, "Stability and control of inductively coupled power transfer systems," *Electric Power Applications, IEE Proceedings -*, vol. 147, no. 1, pp. 37 –43, January 2000.

[19] K. Simonyi, *Theoretische Elekrotechnik*. Leipzig, Berlin, Heidelberg: Johann Ambrosius Barth, 1993.

[20] J. Allmeling and W. Hammer, "Plecs-piece-wise linear electrical circuit simulation for simulink," in *Power Electronics and Drive Systems, 1999. PEDS '99. Proceedings of the IEEE 1999 International Conference on*, 1999.

VI. Biographies

Ruediger Appunn received the diploma in electrical engineering from the Faculty of Electrical Engineering and Information Technology, RWTH Aachen University, Aachen, Germany, in 2008. Since 2008, he has been a researcher with the Institute of Electrical Machines, RWTH Aachen University. His research fields include magnetic levitation, mechatronics and control.

Bjoern Riemer received the diploma in electrical engineering from the Faculty of Electrical Engineering and Information Technology, RWTH Aachen University, Aachen, Germany, in 2009. Since 2009, he has been a researcher at the IEM. His research interests include electromagnetic field calculation as well as simulation and design of electrical machines.

Kay Hameyer (M'96-SM'99) received the M.Sc. degree in electrical engineering from the University of Hannover, Hannover, Germany, and the Ph.D. degree from the University of Technology Berlin, Berlin, Germany. After his university studies, he was with Robert Bosch GmbH, Stuttgart, Germany, as a Design Engineer for permanent-magnet servo motors and electrical energy-supply system components. In 1988, he became a Member of the Staff of the University of Technology Berlin. He was a Full Professor of numerical field computations and electrical machines with the Katholieke Universiteit Leuven, Belgium, until February 2004. In 2005, he was with Poznan University of Technology, Poznan, Poland. He is currently a Full Professor, the Director of the Institute of Electrical Machines, and the holder of the Chair Electromagnetic Energy Conversion at RWTH Aachen University, Aachen, Germany, where he has been the Dean of the Faculty of Electrical Engineering and Information Technology from 2007 till 2009. His research interests include numerical field computation and simulation, design of electrical machines, particularly permanent-magnet excited machines and induction machines, and numerical optimization strategies.